FI SEVIER

Contents lists available at ScienceDirect

# International Journal of Biological Macromolecules

journal homepage: http://www.elsevier.com/locate/ijbiomac



# Facile treatment to fine-tune cellulose crystals in cellulose-silk biocomposites through hydrogen peroxide



Stacy A. Love <sup>a</sup>, Elizabeth Popov <sup>b</sup>, Karleena Rybacki <sup>a</sup>, Xiao Hu <sup>c</sup>, David Salas-de la Cruz <sup>a,d,\*</sup>

- <sup>a</sup> Center for Computational and Integrative Biology, Rutgers University, Camden, NJ, United States of America
- <sup>b</sup> Department of Health Sciences, Rutgers University, Camden, NJ, United States of America
- <sup>c</sup> Department of Physics & Astronomy, Department of Biomedical Engineering, Rowan University, Glassboro, NJ, United States of America
- <sup>d</sup> Department of Chemistry, Rutgers University, Camden, NJ, United States of America

#### ARTICLE INFO

Article history: Received 6 November 2019 Received in revised form 6 January 2020 Accepted 9 January 2020 Available online 10 January 2020

Keywords: Crystallinity Hydrogen peroxide Morphology Cellulose Beta sheet Silk

#### ABSTRACT

The modulation of structural fibrous protein and polysaccharide biopolymers for the design of biomaterials is still relatively challenging due to the non-trivial nature of the transformation from a biopolymer's native state to a more usable form. To gain insight into the nature of the molecular interaction between silk and cellulose chains, we characterized the structural, thermal and morphological properties of silk-cellulose biocomposites regenerated from the ionic liquid, 1-ethyl-3-methylimidazolium acetate (EMIMAc), as a function of increasing coagulation agent concentrations. We found that the cellulose crystallinity and crystal size are dependent on the coagulation agent, hydrogen peroxide solution. The interpretation of our results suggests that the selection of a proper coagulator is a critical step for controlling the physicochemical properties of protein-polysaccharide biocomposite materials.

© 2020 Elsevier B.V. All rights reserved.

## 1. Introduction

Biomaterial research is a rapidly growing interdisciplinary field which connects sciences such as chemistry, physics, engineering, material science and biology. Biopolymers are an expanding class of materials and have been of interest in recent decades due to their abundance, low cost, biocompatibility, and tunable morphological and physicochemical properties [1–5]. They can be used in a multitude of applications such as nature-based electrolyte batteries [6], filters for proteins and heavy metals [7], drug delivery systems [8], and scaffolds for tissue engineering [9]. Numerous types of natural polymers are derived from plants and animals; two relevant examples to this study are structural fibrous proteins and polysaccharides. Structural proteins and polysaccharide polymers interact through hydrophobic interactions and electrostatic interactions [10], and the resulting matrices formed by the mixture can exhibit useful and novel properties [11–14]. However, transforming natural resources from their native state to a more usable form is non-trivial and is the subject of intense scientific scrutiny with significant technical challenges [15].

*E-mail addresses*: sw524@camden.rutgers.edu (S.A. Love), enp27@shp.rutgers.edu (E. Popov), kcr60@scarletmail.rutgers.edu (K. Rybacki), hu@rowan.edu (X. Hu), david.salas@camden.rutgers.edu (D. Salas-de la Cruz).

In biomacromolecule blends, primary and secondary forces play a significant role in the formation and stability of the protein-polysaccharide crystallites such as beta sheets and carbohydrate crystalline structures [2,10,16–18]. The properties of the matrix will depend on how those forces change as a function of specific polymer ratios, types of solvent, and types of coagulation solution. Having the ability to control precise ratios and understanding the effect of fabrication criteria provides a technological approach to the creation of tunable materials with variable but predictable properties [17,19–23].

Biological macromolecules such as cellulose and silk are ideal candidates for the manufacture of blended biomaterials due to their low cost. natural abundance, biodegradability, and biocompatibility [24]. Cellulose, a large linear chain polysaccharide made up of beta (1,4) linked D-glucose units, is the most abundant natural material on earth. Cellulose is a hydrophilic molecule and due to its strong intermolecular hydrogen bonding, it is insoluble in many solvents such as water and most organic solvents. Cellulose is more consolidated in its aggregated state and its crystallinity varies depending upon the source from which it is derived or isolated. Furthermore, when compared to other carbohydrate polymers, cellulose requires higher pressures and temperatures for its molecular aggregated structure to become amorphous. [25,26] The protein, silk fibroin, is hierarchical in its molecular structure and provides less structural rigidity than cellulose. It is a natural fibrous protein produced by insect larvae and delivers properties absent from cellulose such as flexibility. The silk used in this experiment was treated

<sup>\*</sup> Corresponding author.

and originated from the cocoons of the *Bombyx mori* silkworm, and its lesser constituent, sericin, was removed leaving only the insoluble protein, fibroin. Fibroin is the primary structural center of silk and is comprised of antiparallel beta sheet layers with the amino acid sequence (Gly-Ser-Gly-Ala-Gly-Ala) $_{\rm n}$ . This high glycine content and low alanine content allows for a more compact sheet configuration, thus contributing to higher tensile strength often seen in silk.

Typically, protein and polysaccharide biocomposites are processed by dissolution followed by a regenerative phase (coagulation) with a different chemical agent for both of these stages. Each stage provides a pathway to tune the material physico-chemical and morphological properties [27]. Coagulation is a process that combines smaller particles into larger groups and removes organic "impurities" adsorbed onto larger aggregates. Coagulation is a critical fabrication step because the protein can hydrogen bond with the carbohydrate, thus changing the coagulator will change the hydrophobicity and mechanical properties of the blend [28]. In such fabrication methods, solvents are also essential, as they are the driving force behind the dissolution of the silk and cellulose. A poor solvent will significantly affect the miscibility of biocomposites and reduce the mechanical properties [29] and physicochemical properties [30] of the blend. In this investigation, the use of ionic liquid (IL), a molten salt, was applied for dissolving the natural materials. Ionic liquids have been used to dissolve both silk and cellulose without changing their molecular weights [31,32]. Research shows imidazolium-based ionic liquids such as 1-ethyl-3methylimidazolium acetate (EMIMAc) can be used as a viable solvent for silk and cellulose [33]. EMIMAc is liquid at room temperature and can be heated during polymer dissolution without undergoing thermal transition. EMIMAc blended silk and cellulose biocomposites have been shown to have more crystalline polymer morphology compared to other materials of the same polymer composition dissolved in different ionic liquids, thus, inferring a strong influence of ionic liquid type on the structure of silk-cellulose blended materials [33].

Herein, we characterize the structural, thermal and morphological properties of silk-cellulose biocomposites as a function of two main coagulation agent types, water and varying concentrations of hydrogen peroxide, specifically, 1, 2, 5, 10, 15, and 25% (v/v). Selected physicochemical properties were evaluated using a diverse set of techniques including Fourier transform infrared spectroscopy (FTIR), thermal gravimetric analysis (TGA), and X-ray scattering. We found a strong influence in thermal stability among the blended films coagulated in hydrogen peroxide solutions compared to the same blended film coagulated in water. Furthermore, the films coagulated with different hydrogen peroxide concentrations had no varying effect on the protein beta sheet secondary structure formation; however, we observed a strong effect on the cellulose crystallinity, as well as its crystal size.

#### 2. Materials and methods

Avicel microcrystalline cellulose (Techware: Z26578-0) was acquired from Analtech. Before use, the cellulose powder was placed in a vacuum oven at a temperature of 50 °C for 24 h [34]. Silk cocoons of *Bombyx mori* mulberry silkworms were obtained from Treenway Silks (Lakewood, CO). In order to remove the sericin coated on the silk fibers, silkworm cocoons were boiled in a 0.02 M NaHCO<sub>3</sub> (Sigma-Aldrich, USA) solution for 15 min, and then rinsed thoroughly with deionized water three times to remove the sericin completely. The degummed silk was air dried overnight and put into a vacuum oven at room temperature to remove any surface moisture. The ionic liquid, 1-ethyl-3-methylimidazolium acetate, was purchased from Sigma Aldrich and was pretreated before use. The IL was placed in a vacuum oven at 50 °C for 24 h to ensure that the water molecules were removed from the solvent [6,27].

# 2.1. Dissolution and preparation of the protein-polysaccharide biocomposites

In order to create the composite films, the silk and cellulose composition was set to 10% of the total solution weight, while the IL was the remaining 90%. The IL was placed on a stirred hot plate at a temperature of 85 °C. From the 10% of the total solution weight, 10% represent the Mori-silk and 90% the Avicel cellulose. Mori silk-fibroin was added first to the ionic liquid solvent. Upon silk dissolution, microcrystalline Avicel cellulose powder was slowly added then left to sit on the hotplate for 24 h. The newly blended solution was transferred into 3D-printed mold kits of dimensions 12 mm  $\times$  12 mm  $\times$  1 mm; these mold kits were designed by a fabrication laboratory located at Leap Academy University Charter School, a high school located in Camden, NJ affiliated with Rutgers University-Camden. Each mold kit containing the blended solution was placed in 100 mL of the coagulation agent, high purity grade water or various concentrations of hydrogen peroxide. Immersion in the coagulation agent provided the removal of IL from the films, as well as regeneration of the blended polymers. The beakers were then sealed with parafilm and left to sit for 48 h at room temperature. After this coagulation phase, the mold kits containing the polymer blend were removed from their baths and placed in a Teflon evaporating plate. This entire system was transferred to a vacuum oven set at 50 °C for 24 h. After this initial drying stage, the films were removed from their mold kits and sealed in a desiccator for long term storage.

#### 2.2. Characterization

The structural study of the films was conducted using a Bruker's ALPHA-Platinum ATR-FTIR Spectrometer with Platinum-Diamond sample module at a spectrum between 4000 cm<sup>-1</sup> to 400 cm<sup>-1</sup>. 128 background scans were performed along with 32 sample scans in 6 different locations of the film. Fourier self-deconvolution was used to study the amide I and II regions (1595 cm<sup>-1</sup>-1705 cm<sup>-1</sup>). The Lorentzian line shape, with a 25.614 cm<sup>-1</sup> half-bandwidth and a noise reduction factor of 0.3, was used for performing deconvolution. Gaussian profiles were utilized to allow for fitting results and then integrated to find the area relating to a specific wavenumber. These two fitting functions were repeated 4 times to calculate the standard deviation. All analyses were performed using Opus 7.2 software. The data was normalized from 4000 cm<sup>-1</sup> to 400 cm<sup>-1</sup> using min-max normalization. Thermogravimetric analysis (TGA) was then performed using TA Instruments Discovery TGA system with 5 mg samples. All samples were under a nitrogen gas purge of 25 mL/min and started at 30 °C. They underwent an isothermal period of 1 min and then ramped to 10 °C per minute to 600 °C. Step transition analyses and derivative plots were utilized to determine the onset of decomposition ( $T_{Onset}$ ), the weight-loss percentage of the sample, and the temperature which corresponds to the decomposition of the sample at the highest rates ( $T_{\Delta Max}$ ). Finally, the morphological studies were conducted using a multi-angle X-ray scattering system (DEXS) at the University of Pennsylvania under standard room conditions. The Xeuss 2.0 by XENOCS has a Cu X-ray source, computer controlled focusing and transmission incident sample geometries, a 1 M pixel Pilatus detector (2D), and a smaller detector for simultaneous SAXS and WAXS. Only the WAXS data is presented in this paper. A full flux collimation was used with a slit of 1.2 mm  $\times$  1.2 mm. Each sample was run for 300 s. The intensity reported is not absolute intensity and, thus, is reported in arbitrary units (a.u.). All films were taped to a sample-holder and placed in a cabin under normal atmospheric pressure during X-ray scattering characterization. The X-ray scattering profiles were evaluated using Foxtrot 3.4.9; the isotropic 2-D scattering patterns were azimuthally integrated to yield intensity versus scattering vector. Azimuthal integration was used for the WAXS plots and was graphed at  $2\theta^{\circ}$  to calculate the crystal size using the Scherrer equation. Three different methods for determining the full width at half maximum (FWHM) on the software, OriginPro 2019, was applied and the mean average crystal size was obtained for each biomaterial film for comparison within the sample set.

#### 3. Results and discussion

Qualitatively, the regenerated films exhibited a hard and brittle quality for each film composed of 90% cellulose and 10% silk dissolved from the solvent, EMIMAc, and coagulated in two separate bath types, water and various concentrations of hydrogen peroxide of 1, 2, 5, 10, 15, and 25% (v/v). Results from different characterization tests showed a positive correlation between higher concentrations of hydrogen peroxide solution and morphological crystallinity of the blended biomacromolecule film, specifically cellulose crystal size.

#### 3.1. Structural analysis

Normalized data from Fourier transform infrared spectroscopy (FTIR) was used to identify the functional groups and fingerprint regions of each film, thus providing information on the integrity of the overall polymer blend. Fig. 1 shows absorbance peaks in 3600–3000 cm<sup>-1</sup>, 3000–2750 cm<sup>-1</sup>, and 1180–930 cm<sup>-1</sup> regions are represented by cellulose -OH, -CH, and -C-O stretching modes, respectively, within each sample. Fig. 2 shows the silk's amide I  $(1720-1600 \text{ cm}^{-1})$  [35] and amide II  $(1590-1500 \text{ cm}^{-1})$  regions. This demonstrates that the biocomposites are well blended. Fourier Self-Deconvolution was used to analyze the silk's amide I and amide II regions for various secondary structure percentages, specifically side chains,  $\beta$ -sheets, random coils,  $\alpha$ -helices, and turns. Fig. 3 shows subtle correlations between hydrogen peroxide concentration and secondary structure percentages of these regions. The results show that the hydrogen peroxide concentration as the sole variable does not affect silk crystalline structures, i.e.  $\beta$ -sheet formation. However, there seems to be a small effect on the formation of  $\alpha$ -helices as function of hydrogen peroxide concentration. The data shows that the alpha helices content seem to be linearly depend on hydrogen peroxide content. This effect is apparent at higher coagulation concentrations. This means that at some point, the silk molecular chains become assembled, thus resulting in an increased change of helical structure formation from a random formation shown at lower concentrations of hydrogen peroxide. This seems logical but when we apply the standard deviation, the results show again a subtle change as a function of hydrogen peroxide content.

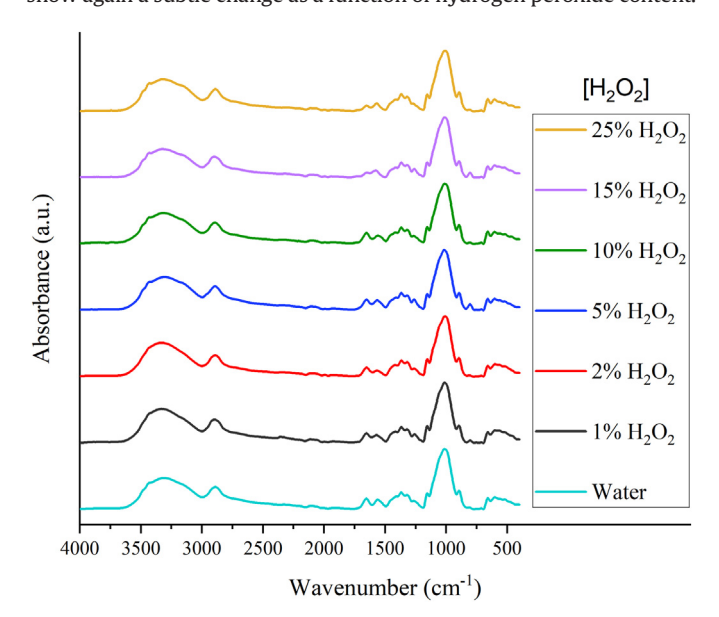
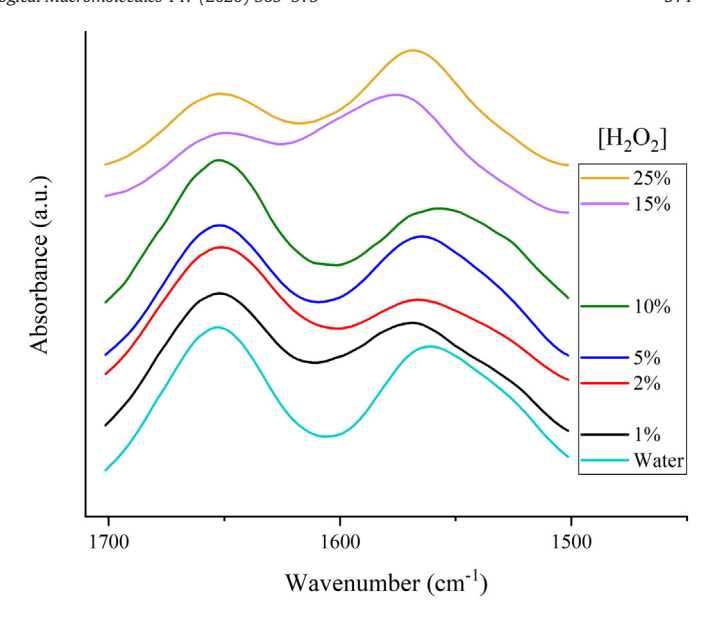


Fig. 1. Normalized spectra of seven samples made with different coagulation baths (listed on legend). All sampled are composed of 90% cellulose-10% silk and dissolved in EMIMAc.



**Fig. 2.** For the analyzation of protein secondary structure percentages; zoomed in spectra of the Amide *I* and II regions of seven samples made with different coagulation baths (listed on legend). All sampled are composed of 90% cellulose-10% silk and dissolved in **FMIMAC** 

#### 3.2. Thermogravimetric analysis

The thermal properties were analyzed by the Thermogravimetric analyzer (TGA) to determine each samples' decomposition in weight over time as the temperature increases from 30 °C to 600 °C. Fig. 4 shows a thermogram with a range of temperature onsets between 292.0 °C and 298.3 °C for various concentrations of hydrogen peroxide-coagulated samples, while the data for the same film, except coagulated in pure water instead of hydrogen peroxide, showed a temperature onset at 209.5 °C. Compared to the films coagulated with hydrogen peroxide solutions, the water-coagulated film's onset temperature decreased at least 82.5°. The percent mass decomposition was also evaluated for each sample; 71.5% of the sample coagulated in water was loss, while a range of 61.9% to 58.4% mass loss was shown

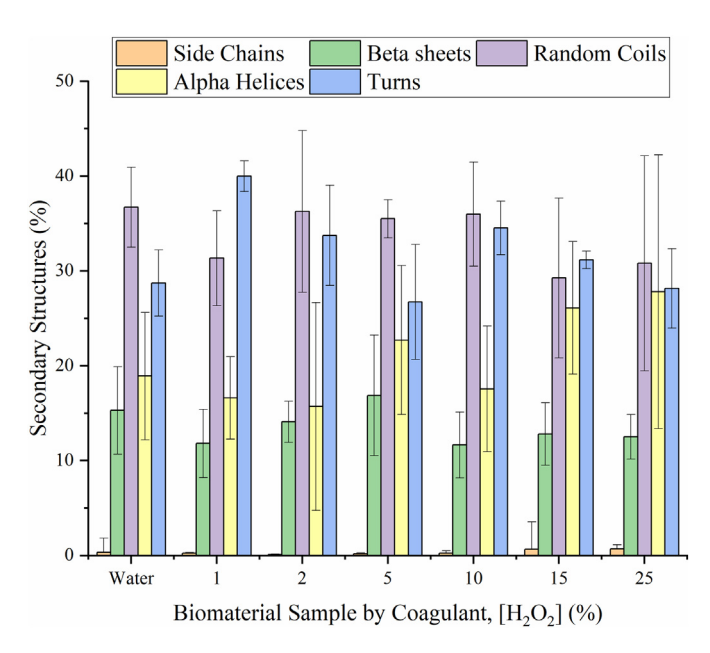


**Fig. 3.** Secondary structure percentages of 90% cellulose-10% silk samples from different coagulation baths.

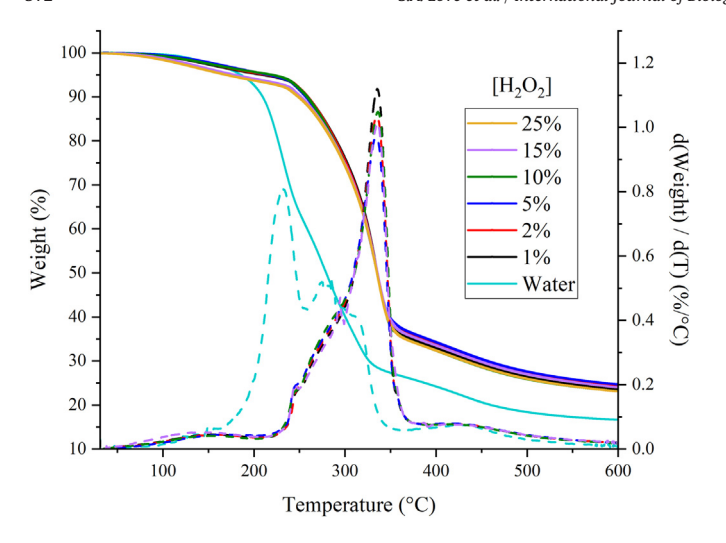


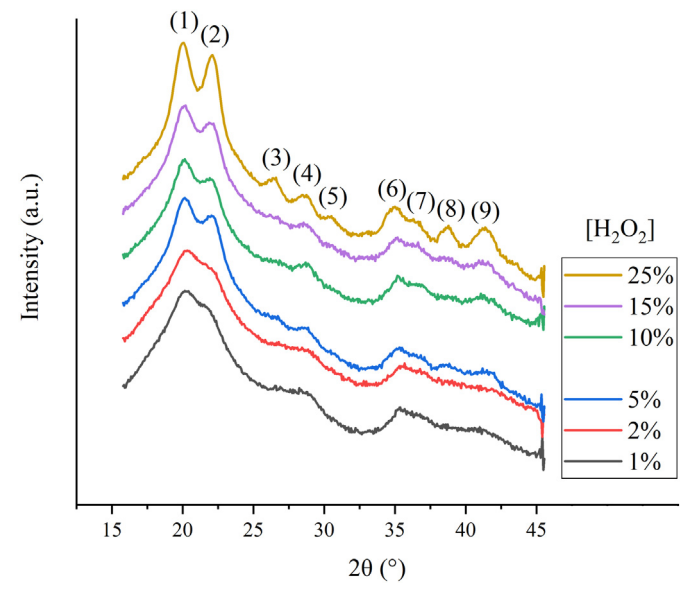
**Fig. 4.** Thermogram showing decomposition rates of seven samples of different coagulation baths (listed on legend) with their derivatives (dashed lines). 90% cellulose-10% silk. dissolved in EMIMAc.

in the hydrogen peroxide-coagulated films, confirming less thermal decomposition for the hydrogen peroxide-coagulated films compared to the film coagulated in water. Fig. 4 also shows the data's derivative (dashed lines) over increasing temperature; a trimodal peak was observed with a max peak height of 230 °C in the water-coagulated film's thermogram, affirming that there exists at least two to three stages of high decomposition rates in this material, thus showing the various formations of different polymer interfaces. Previously, we demonstrated, computationally, that for a protein-polysaccharide blend the interfaces between chains break down easily, so that a lot of small "pure" crystals are released. Immediately after initial decomposition, single chains are released from these interfaces and begin to decompose. Furthermore, the crystalline regions survive for a bit longer before melting and decomposing in a similar way [27]. Our data results are similar to such predictions.

In continuation with the analysis, each biocomposite film coagulated in hydrogen peroxide showed a high decomposition rate at around 336 °C with a small shoulder at 275 °C. This demonstrates that films coagulated in hydrogen peroxide are more thermally stable than the same type of film coagulated in water. The decomposition seen at the small shoulder of the thermogram is due to fewer interfaces between polymer chains for all biocomposites coagulated with hydrogen peroxide solutions. This is because it takes much less cohesive energy to break these interfaces compared to the actual disruption of the polymer chains themselves. Also, observations from the data point out that the thermal stability is independent of varying concentrations of hydrogen peroxide. In other words, a 1% hydrogen peroxide-coagulated film showed similarly high thermal stability to a film coagulated in as much as 25% hydrogen peroxide.

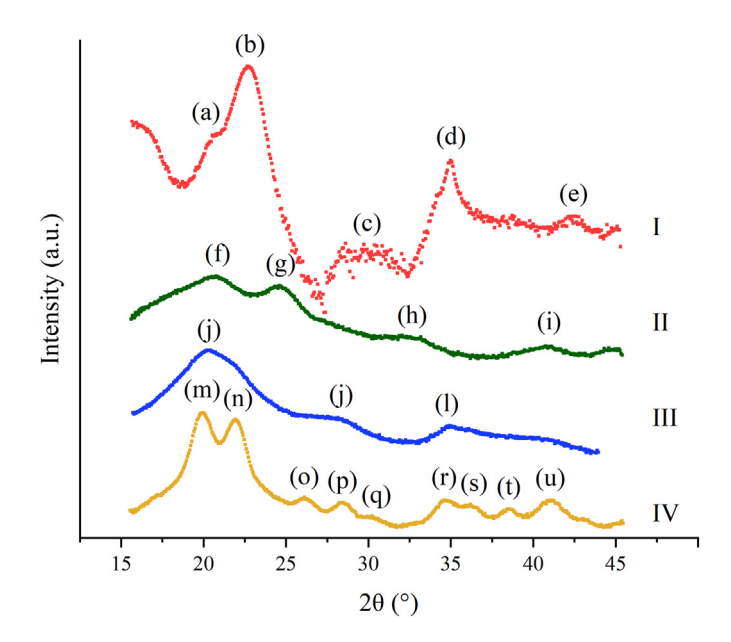
#### 3.3. Morphological analysis

Fig. 5 shows the X-ray scattering wide angle region in the 15 to  $45^{\circ}$  20 range for the various silk-cellulose films coagulated in various concentrations of hydrogen peroxide. We initiated our morphological investigation by analyzing both qualitative and quantitative information. Qualitatively, our results demonstrated that the X-ray scattering peak intensities increase as the coagulation agent concentration of hydrogen peroxide solution increases. The typical sharp crystallization reflection, which are characteristics of native microcrystalline Avicel cellulose  $I_{\beta}$  (see Fig. 6), are not observed in the biocomposites that were coagulated with lower concentrations of hydrogen peroxide solution. Instead, these biocomposites show a broader region which is indicative of an amorphous structure. The amorphous structure gradually transforms into a



**Fig. 5.** Wide angle scattering profiles of different biocomposites coagulated in various concentrations of hydrogen peroxide, 90% cellulose-10% silk, dissolved in EMIMAc.

semi-crystalline morphology as indicative of the typical peak sharpness. These peaks contain the signature of both silk and cellulose materials. In Fig. 6, we demonstrate that the morphology of pure Avicel cellulose can be transformed from a crystalline cellulose  $I_{\beta}$  structure to an amorphous structure when regenerated in EMIMAc and coagulated with water. In addition, this film can be further changed from amorphous to a semi-crystalline cellulose II structure by changing the coagulation agent from water to 25% hydrogen peroxide. These results demonstrated that the crystallinity of the cellulose can be influenced by the ionic liquid solvent and by the type of coagulation agent; using a solution of hydrogen peroxide changes the cellulose crystallinity of the product. Tables 1 and 2 shows the quantitative data for all biocomposites and for native samples, respectively. The data is presented both in scattering vector,



**Fig. 6.** Wide angle scattering profiles of native and regenerated polymer samples: (I) Avicel microcrystalline cellulose, (II) *Bombyx Mori* Silk, (III) regenerated 100% cellulose coagulated in water, (IV) regenerated 100% cellulose coagulated in 25% hydrogen peroxide.

q, and 2 $\theta$ . In addition, the correlation distance, d, is shown and is as calculated by  $d=2\pi/q$ .

To understand the morphological changes in our biocomposite films, let's first look at a native material. Four distinct contributions are observed in Avicel cellulose. The first two peaks in  $2\theta$ , a = 20.47 and b=22.71 are related to the monoclinic unit cell of cellulose  $I_{\beta}$  equatorial lattice planes. This corresponds to the 102 and 200 reflections, respectively [36,37]. Upon dissolution in ionic liquid and coagulation in water, the cellulose I<sub>B</sub> morphology changed from crystalline to amorphous. The two reflections observed in Avicel cellulose I<sub>B</sub> turned into one reflection,  $2\theta = 20.26$ . However, upon coagulating the Avicel cellulose with 25% hydrogen peroxide, the cellulose I<sub>B</sub> was modified to cellulose II [36,38]. In this case, we observed multiple reflections for which the peak (m) and (n), Fig. 6, are related to the 110 and 200 reflections typical for this material; the other higher angle reflections are indicative of the crystalline structure periodicity. Analyzation of our results further confirm that a solution of hydrogen peroxide as a coagulation agent can induce morphological changes in the cellulose structure.

In terms of the biocomposite films, we observed reflections similar to that of the cellulose II. In this case and based on the FTIR results, we must remember that we also have silk molecules in the biocomposites, so the typical cellulose II reflections are slightly skewed. The results show two main reflections at  $2\theta=20.01$  and 22.10; the location of these two reflections barely changes as a function of hydrogen peroxide. However, their intensity linearly increases. The change in peak intensity is related to changes in crystallinity. To understand crystallization changes, the crystal size from our biocomposite films were determined using the Scherrer equation using both the 110 and 200 reflections,

$$\tau = \frac{K\lambda}{\beta \cos \theta}$$

Dools 1%

where  $\tau$  is the mean size of the crystal, K is the dimensionless shape factor (0.94),  $\lambda$  is the wavelength of the X-ray,  $\beta$  represents the FWHM in radians, and  $\cos\theta$  is the Bragg angle. Table 3 shows the Scherrer equation crystal size results. The crystal size ( $\tau$ ) associated with the scattering angle of 20 in the biomaterial data shows a positive correlation with higher concentrations of hydrogen peroxide as the coagulation agent. The reflection at 110 shows a better relationship than at 200 probably

**Table 1**X-ray scattering quantitative peaks from Fig. 5 (90% cellulose-10% silk biocomposites coagulated in various concentration of hydrogen peroxide).

5%

Реак	1%			2%			5%		
	q (nm <sup>-1</sup> )	2θ°	d (nm)	q (nm <sup>-1</sup> )	2θ°	d (nm)	q (nm <sup>-1</sup> )	2θ°	d (nm)
1	14.34	20.24	0.44	14.39	20.31	0.44	14.27	20.14	0.44
2	15.34	21.67	0.41	15.52	21.93	0.4	15.62	22.08	0.4
3	-	-	-	-	-	-	18.73	26.54	0.34
4	20.2	28.67	0.31	20.02	28.4	0.31	20.21	28.68	0.31
5	0	-	-	-	-	-	-	-	-
6	24.72	35.26	0.25	24.83	35.43	0.25	24.69	35.23	0.25
7	-	-	-	25.84	36.92	0.24	-	-	-
8	-	-	-	-	-	-	26.99	38.63	0.23
9	28.6	41.03	0.22	29	41.63	0.22	28.86	41.43	0.22
	10%		15%			25%			
Peak	10%			15%			25%		
Peak	$\frac{10\%}{q}$ $(nm^{-1})$	2θ°	d (nm)	q	2θ°	d (nm)	$\frac{25\%}{q}$ (nm <sup>-1</sup> )	2θ°	d (nm)
Peak 1	q	2θ° 20.11		q			q		(nm)
	q (nm <sup>-1</sup> )		(nm)	q (nm <sup>-1</sup> )		(nm)	q (nm <sup>-1</sup> )		(nm)
1	q (nm <sup>-1</sup> ) 14.25	20.11	(nm) 0.44	q (nm <sup>-1</sup> ) 14.23	20.09	(nm) 0.44	q (nm <sup>-1</sup> ) 14.18	20.01	(nm) 0.44
1 2	q (nm <sup>-1</sup> ) 14.25	20.11	(nm) 0.44	q (nm <sup>-1</sup> ) 14.23 15.52	20.09 21.93	(nm) 0.44 0.4	q (nm <sup>-1</sup> ) 14.18 15.64	20.01 22.1	(nm) 0.44 0.4
1 2 3	q (nm <sup>-1</sup> ) 14.25 15.52	20.11 21.93 -	(nm) 0.44 0.4 -	q (nm <sup>-1</sup> ) 14.23 15.52 18.54	20.09 21.93 26.26	(nm) 0.44 0.4 0.34	q (nm <sup>-1</sup> ) 14.18 15.64 18.66	20.01 22.1 26.44	(nm) 0.44 0.4 0.34
1 2 3 4	q (nm <sup>-1</sup> ) 14.25 15.52	20.11 21.93 -	(nm) 0.44 0.4 -	q (nm <sup>-1</sup> ) 14.23 15.52 18.54	20.09 21.93 26.26 28.48	(nm) 0.44 0.4 0.34	q (nm <sup>-1</sup> ) 14.18 15.64 18.66 20.16	20.01 22.1 26.44 28.61	0.44 0.4 0.34 0.31
1 2 3 4 5	q (nm <sup>-1</sup> ) 14.25 15.52 - 20.24	20.11 21.93 - 28.73	(nm) 0.44 0.4 - 0.31	q (nm <sup>-1</sup> ) 14.23 15.52 18.54 20.07	20.09 21.93 26.26 28.48	0.44 0.4 0.34 0.31	q (nm <sup>-1</sup> ) 14.18 15.64 18.66 20.16 21.44	20.01 22.1 26.44 28.61 30.47	(nm) 0.44 0.4 0.34 0.31 0.29
1 2 3 4 5 6	q (nm <sup>-1</sup> ) 14.25 15.52 - 20.24 - 24.69	20.11 21.93 - 28.73 - 35.23	(nm) 0.44 0.4 - 0.31 - 0.25	q (nm <sup>-1</sup> ) 14.23 15.52 18.54 20.07 - 24.63	20.09 21.93 26.26 28.48 - 35.13	(nm) 0.44 0.4 0.34 0.31 - 0.26	q (nm <sup>-1</sup> )  14.18 15.64 18.66 20.16 21.44 24.5	20.01 22.1 26.44 28.61 30.47 34.95	(nm) 0.44 0.4 0.34 0.31 0.29 0.26

**Table 2**X-ray scattering quantitative peaks from Fig. 6 for native samples and 100% regenerated cellulose samples.

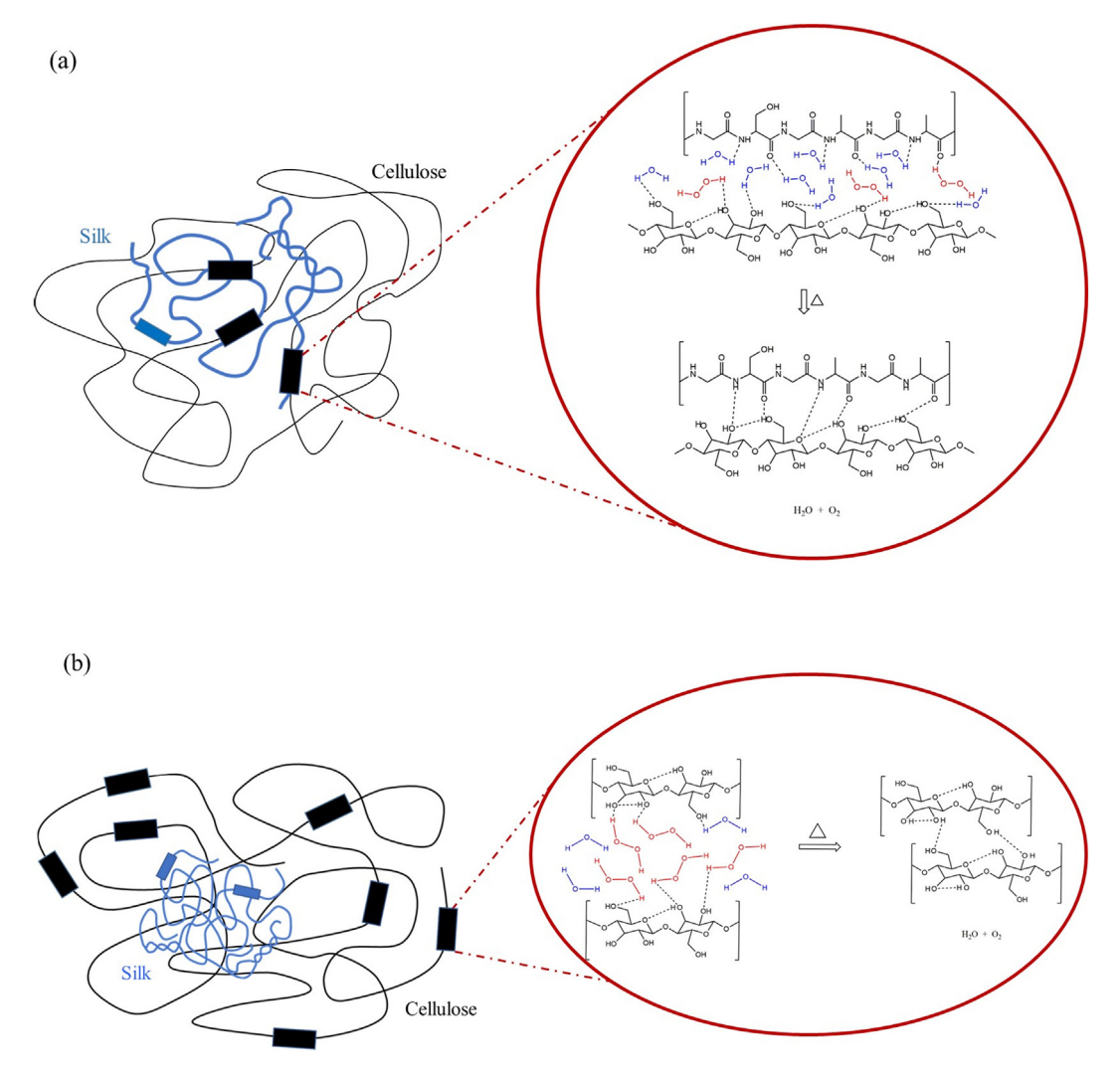
Peak $q (nm^{-1})$	2θ (°)	d (nm)
<b>a</b> 14.50	20.47	0.43
<b>b</b> 16.07	22.71	0.39
<b>c</b> 20.95	29.76	0.30
<b>d</b> 24.50	34.95	0.26
<b>e</b> 29.33	42.14	0.21
<b>f</b> 14.60	20.61	0.43
<b>g</b> 17.36	24.56	0.36
<b>h</b> 22.63	32.21	0.28
i 28.40	40.74	0.22
<b>j</b> 14.35	20.26	0.44
<b>k</b> 19.79	28.07	0.32
l 24.46	34.88	0.26
<b>m</b> 14.11	19.91	0.45
<b>n</b> 15.52	21.93	0.40
o 18.45	26.13	0.34
<b>p</b> 20.00	28.38	0.31
<b>q</b> 21.25	30.19	0.30
r 24.28	34.63	0.26
s 25.34	36.19	0.25
t 26.91	38.51	0.23
<b>u</b> 28.60	41.03	0.22

due to the interference from the silk. The crystal size for the 110 reflection increases from 3.01 nm to 4.87 nm and for the 200 reflection from 4.59 nm to 5.04 nm. In comparison, the Avicel cellulose  $I_{\beta}$  crystal size calculated from the Scherrer equation using the reflection at 200 is 4.25 nm and for the 100% regenerated cellulose coagulated with 25% hydrogen peroxide is 5.12 nm. The results of our biomaterials are within the native samples ranges indicating that both the silk and cellulose are interacting at the nano level, as expected. Based on these results it may be concluded that the cellulose crystal size increases as a function of hydrogen peroxide content.

Scheme 1 shows a coagulation mechanism of hydrogen peroxide after the removal of ionic liquid. However, before this salting-out effect, hydrogen peroxide and water molecules coexist within the system containing the dissolved silk fibroin, cellulose, and ionic liquid. These water and hydrogen peroxide molecules quickly hydrate the protein and cellulose chains. This leads to the formation of stable structures resulting from the formation of protein secondary structures and interactions with cellulose; these interactions involve hydrogen bonds, electrostatic interactions, and covalent bonds [39,40]. The interaction between silk, cellulose, and the solvent may promote and stabilize its morphological structure to lower conformation energies, resulting from the hydrogen bonds with water and hydrogen peroxide. As hydrogen peroxide content increases, the hydrogen peroxide molecules prefer to hydrogen bond with the cellulose rather than the silk, resulting in a metastable polymer blend form due to a lack of ions, further promoting solvation. Upon drying, hydrogen peroxide is converted into oxygen gas and water molecules. This chemical reaction collapses the polymer chains in situ, resulting in changes in the cellulose crystallinity; specially the cellulose crystal size. As a result, the morphology and physicochemical properties of the material will depend on the solvent composition and

**Table 3** Crystal size results  $(\tau)$  of biomaterial samples; labeled by coagulation concentration agent, obtained from the Scherrer equation.

Sample	Peak 1			Peak 2	Peak 2		
	2q°	τ (nm)	SD	2q°	τ (nm)	SD	
1	20.28	3.01	0.41	_	-		
2	20.44	2.93	0.45	_	_		
5	20.15	3.55	0.21	22.11	4.59	0.49	
10	20.14	3.61	0.25	22.02	4.48	0.40	
15	20.17	3.84	0.23	21.95	4.70	0.33	
25	20.06	4.87	0.34	22.10	5.04	0.55	



**Scheme 1.** Regeneration mechanism for biocomposite coagulated in (a) 1% hydrogen peroxide and (b) 25% hydrogen peroxide. A higher concentration of coagulating agent prefers to hydrogen bond with the cellulose *hydroxide* group which aligns the molecules into crystalline structures.

volume spacing between polymer chains [41,42]. In other words, any perturbation in the metastable system will cause changes in the material formation, dictating final properties. Moreover, the cellulose could act as a nucleating agent to increase the nucleation and overall crystallization rate leading to an increase in crystallites [43].

#### 4. Conclusion

To summarize, in this study, using EMIMAc and two types of coagulation agents (water and solutions of various hydrogen peroxide concentrations) a cellulose-silk biocomposite was regenerated and characterized. Regarding the two polar coagulation agents, there is a strong influence on the thermal stability seen within the film coagulated in hydrogen peroxide compared to the film coagulated in water. According to data from FTIR, hydrogen peroxide seems to have subtle effects on silk crystalline secondary structures in the blended biomaterial. However, higher concentrations of hydrogen peroxide as the coagulation agent appeared to enhance the overall structural influence on cellulose in the blended materials. This was demonstrated by an increase in thermal degradation temperature and stability as well as by a positive correlation to cellulose crystal size demonstrated via X-ray scattering. It may be concluded that hydrogen peroxide can be used to fine-tune cellulose crystals within a silk-cellulose blended film dissolved from ionic liquids. Further research will look at other morphological and physicochemical property impacts by comparing various types of polymer ratios of silk to cellulose and ionic liquid types to different hydrogen peroxide concentrations.

#### **CRediT authorship contribution statement**

Stacy A. Love:Formal analysis, Validation, Investigation, Writing original draft, Visualization.Elizabeth Popov:Investigation.Karleena Rybacki:Investigation, Software.Xiao Hu:Conceptualization, Methodology, Funding acquisition, Writing - review & editing.David Salas-de la Cruz:Conceptualization, Methodology, Validation, Supervision, Project administration, Funding acquisition, Writing - review & editing, Resources.

## **Declaration of competing interest**

All authors declare no financial and/or personal relationships with any person or organization which may have inappropriately influenced the work in this study.

### Acknowledgments

The authors are grateful for financial support from NSF-DMR-RUI (1809354 and 1809541): National Science Foundation Division of Material Research Biomaterial Program, United State of America, NSF-REU (DBI-1559868): National Science Foundation Division of Biological

Infrastructure Research Experiences for Undergraduate Sites, United States of America, Rutgers-Camden Arts and Sciences Start-up Package, State of NJ ELF Grant and The Center for Computational and Integrative Biology TA Funds, DEXS System is supported by NSF-MRSEC (17-20530) National Science Foundation Division of Material Research, United States of America, NSF-MRI (17-25969): National Science Foundation Division of Material Science Major Reseach Instrumentation Program, United States of American, ARO DURIP (W911NF-17-1-02822): Army Research Office Defense University Research Instrumentation Program, United States of America, and the University of Pennsylvania. A special thank you to Dr. Paul Heiney, Department of Physics and Astronomy at the University of Pennsylvania, and Benjamin Paren, Ph.D. student at the University of Pennsylvania, for technical support and training on the DEXS system.

#### References

- [1] J. Yin, S. Luan, Opportunities and challenges for the development of polymer-based biomaterials and medical devices, Regenerative Biomater. 3 (2) (2016) 129-135.
- M. Metzke, Z. Guan, Structure-property studies on carbohydrate-derived polymers for use as protein-resistant biomaterials, Biomacromolecules 9 (1) (2008) 208-215.
- S. Kumar, et al., Studies of carbon dioxide capture on porous chitosan derivative, J. Dispers. Sci. Technol. 37 (2) (2016) 155-158.
- X. Zhang, et al., Synthesis and characterization of xylan grafted with polyethylene glycol in ionic liquid and their use as moisture-absorption/retention biomaterials, Macromol. Mater. Eng. 301 (3) (2016) 287-295.
- D. Mawad, A. Lauto, G.G. Wallace, Conductive polymer hydrogels, Polymeric Hydrogels as Smart Biomaterials, Springer 2016, pp. 19-44.
- B. Blessing, et al., Morphology and ionic conductivity relationship in silk/cellulose biocomposites, Polym. Int. 68 (9) (2019) 1580-1590.
- W. Zhou, et al., Preparation of electrospun silk fibroin/cellulose acetate blend nanofibers and their applications to heavy metal ions adsorption, Fibers Polym. 12 (4) (2011) 431-437.
- [8] L. Lamboni, et al., Silk sericin: a versatile material for tissue engineering and drug delivery, Biotechnol. Adv. 33 (8) (2015) 1855-1867.
- [9] H.O. Barud, et al., Preparation and characterization of a bacterial cellulose/silk fibroin sponge scaffold for tissue regeneration, Carbohydr. Polym. 128 (2015) 41-51.
- [10] G. Freddi, et al., Silk fibroin/cellulose blend films: preparation, structure, and physical properties, J. Appl. Polym. Sci. 56 (12) (1995) 1537-1545.
- L. Zhou, et al., Preparation and characterization of transparent silk fibroin/cellulose blend films, Polymer 54 (18) (2013) 5035-5042.
- [12] P. Wongpanit, et al., Preparation and characterization of chitin whisker-reinforced silk fibroin nanocomposite sponges, Eur. Polym. J. 43 (10) (2007) 4123–4135.
- C.D. Tran, T.M. Mututuvari, Cellulose, chitosan and keratin composite materials: facile and recyclable synthesis, conformation and properties, ACS Sustain. Chem. Eng. 4 (3) (2016) 1850-1861.
- R. Boy, et al., Novel cellulose-collagen blend biofibers prepared from an amine/salt solvent system, Int. J. Biol. Macromol. 92 (2016) 1197-1204.
- M. Muskovich, C.J. Bettinger, Biomaterials-based electronics: polymers and interfaces for biology and medicine, Adv. Healthc. Mater. 1 (3) (2012) 248-266.
- Levy, I., et al., Recombinant cellulose crosslinking protein: a novel papermodification biomaterial. Cellulose. 9(1): p. 91-98.
- J.-F. Su, et al., Structure and properties of carboxymethyl cellulose/soy protein isolate blend edible films crosslinked by Maillard reactions, Carbohydr. Polym. 79 (1)
- [18] M. Tomczyńska-Mleko, K. Terpiłowski, S. Mleko, Physicochemical properties of cellulose/whey protein fibers as a potential material for active ingredients release, Food Hydrocoll. 49 (2015) 232-239.

- [19] X. Hu, et al., Protein-based composite materials, Mater, Today 15 (5) (2012) 208-215.
- X. Hu, et al., Stability of silk and collagen protein materials in space, Sci. Rep. (3) (2013) 3428
- [21] F. Wang, et al., Comparative studies of regenerated water-based Mori, Thai, Eri, Muga and tussah silk fibroin films, J. Therm. Anal. Calorim. 122 (3) (2015) 1069-1076
- [22] T. Vu. et al., Comparative study of ultrasonication-induced and naturally selfassembled silk fibroin-wool keratin hydrogel biomaterials, Int. I. Mol. Sci. 17 (9) (2016) 1497.
- [23] I. Stanton, et al., Structure-property relationships of blended polysaccharide and protein biomaterials in ionic liquid, Cellulose 24 (4) (2017) 1775–1789.
- A. Sionkowska, Current research on the blends of natural and synthetic polymers as new biomaterials, Prog. Polym. Sci. 36 (9) (2011) 1254–1276.
- U.P. Agarwal, et al., Effect of sample moisture content on XRD-estimated cellulose crystallinity index and crystallite size, Cellulose 24 (5) (2017) 1971-1984.
- [26] U.P. Agarwal, et al., Probing crystallinity of never-dried wood cellulose with Raman spectroscopy, Cellulose 23 (1) (2016) 125-144.
- A. Hadadi, et al., A hierarchical model to understand the processing of polysaccharides/protein-based films in ionic liquids, Biomacromolecules 19 (10) (2018) 3970-3982
- H.F. Oldenkamp, J.E. Vela Ramirez, N.A. Peppas, Re-evaluating the importance of carbohydrates as regenerative biomaterials, Regenerative Biomater. 6 (1) (2018) 1–12.
- A. Isogai, R.H. Atalla, Dissolution of cellulose in aqueous NaOH solutions, Cellulose 5 (4) (1998) 309–319.
- Q. Wang, et al., Effect of various dissolution systems on the molecular weight of regenerated silk fibroin, Biomacromolecules 14 (1) (2013) 285-289.
- H. Zhang, et al., 1-Allyl-3-methylimidazolium chloride room temperature ionic liguid: a new and powerful nonderivatizing solvent for cellulose, Macromolecules 38 (20) (2005) 8272-8277.
- Q. Wang, et al., Investigation of rheological properties and conformation of silk fibroin in the solution of AmimCl, Biomacromolecules 13 (6) (2012) 1875-1881.
- J. Stanton, et al., Impact of ionic liquid type on the structure, morphology and properties of silk-cellulose biocomposite materials, Int. J. Biol. Macromol. 108 (2018) 333-341
- Z. Liu, et al., Characterization of the regenerated cellulose films in ionic liquids and rheological properties of the solutions, Mater. Chem. Phys. 128 (1-2) (2011) 220-227
- [35] A.K. Biswal, et al., Identification of the secondary structure of protein isolated from deoiled cake flour of Mahua (Madhuca Latifolia), Mater. Today Proceedings 9 (2019) 605-614.
- C.M. Lee, et al., Cellulose polymorphism study with sum-frequency-generation (SFG) vibration spectroscopy: identification of exocyclic CH 2 OH conformation and chain orientation, Cellulose 20 (3) (2013) 991-1000.
- A. Lewis, et al., Macromolecular interactions control structural and thermal properties of regenerated tri-component blended films, Int. J. Mol. Sci. 17 (12) (2016)
- L.P. Novo, et al., Subcritical water: a method for green production of cellulose nanocrystals, ACS Sustain. Chem. Eng. 3 (11) (2015) 2839-2846.
- U.-J. Kim, et al., Three-dimensional aqueous-derived biomaterial scaffolds from silk fibroin, Biomaterials 26 (15) (2005) 2775-2785.
- S. Shang, L. Zhu, J. Fan, Intermolecular interactions between natural polysaccharides and silk fibroin protein, Carbohydr. Polym. 93 (2) (2013) 561-573
- J. Stanton, et al., Morphological and Thermal Properties of Silk/Cellulose-Based Biomaterial as a Function of Ionic Liquid Type, In preparation 2017.
- H.J. Jin, et al., Water-stable silk films with reduced β-sheet content, Adv. Funct. Mater. 15 (8) (2005) 1241-1247.
- L. Liu, et al., Biomimicking the structure of silk fibers via cellulose nanocrystal as β-
- sheet crystallite, RSC Adv. 4 (27) (2014) 14304-14313.